Simulating the freeze-thaw and buried ice melting process of the Longbasaba moraine dam (Himalayas) based on the heat transfer module of COMSOL Multiphysics from 1959 to 2100

Wang Jia[1], Wang Xin[1], Zhang Yanlin[1], Ran Weijie[1], Zhang Yong[1], Wei Junfeng[1], Liu Qiao[2], and Lei Dongyu[1]

[1]Hunan University of Science and Technology
[2]Institute of Mountain Hazards and Environment, Chinese Academy of Sciences

November 16, 2022

Abstract

Permafrost degradation poses an increasingly serious threat of glacial lake outburst floodings (GLOFs) in the Tibetan Plateau. It is therefore of great practical significance to analyze the freeze-thaw state in moraine dams and associated impacts on dam stability. We simulated the soil temperature of the Longbasaba moraine dam based on the heat transfer module of COMSOL Multiphysics. The results show that the soil temperature of the moraine dam can be adequately simulated using the COMSOL Multiphysics heat transfer module and the simulated temperature values are generally consistent with the observed trends, yielding root mean square errors (RMSEs) less than 1.58 and Nash-Sutcliffe efficiency coefficients (NSEs) between 0.66 and 0.93. The average annual increase of the active layer depth was 0.026 m/a from 1959 to 2020. The buried ice inside the moraine dam was evidently melting and the maximum buried ice thawing depth under scenarios SSP1-2.6, SSP2-4.5, and SSP5-8.5 in CMIP6 (Coupled Model Intercomparison Project Phase 6) is expected to be 11.3 m, 18.4 m, and 23.5 m, respectively, by the end of the century, which indicates a continuous deterioration of the moraine dam stability.

Hosted file

`essoar.10512105.1.docx` available at https://authorea.com/users/524644/articles/595524-simulating-the-freeze-thaw-and-buried-ice-melting-process-of-the-longbasaba-moraine-dam-himalayas-based-on-the-heat-transfer-module-of-comsol-multiphysics-from-1959-to-2100

Simulating the Freeze-thaw and Buried Ice Melting Process of the Longbasaba Moraine Dam (Himalayas) Based on the Heat Transfer Module of COMSOL Multiphysics from 1959 to 2100

Jia Wang[1], Xin Wang[1*], Yanlin Zhang[1], Weijie Ran[1], Yong Zhang[1], Junfeng Wei[1], Qiao Liu[2], Dongyu Lei[1]

[1] School of Earth Science and Geospatial Information Engineering, Hunan University of Science and Technology, Xiangtan, China.

[2] Institute of Mountain Hazards and Environment, Chinese Academy of Sciences, Chengdu, China.

Corresponding author: Xin Wang (wangx@hunst.edu.cn)

Key Points:

- A moraine dam soil temperature field inside was soundly simulated with root mean square errors less than 1.58 °C.
- Annual active layer depth increased from 1959–2020 with an average increase rate of 0.026 m/a.
- The buried ice inside moraine dam is melting acceleratively under CMIP6 scenarios, which would deteriorate its stability.

Abstract

Permafrost degradation poses an increasingly serious threat of glacial lake outburst floodings (GLOFs) in the Tibetan Plateau. It is therefore of great practical significance to analyze the freeze-thaw state in moraine dams and associated impacts on dam stability. We simulated the soil temperature of the Longbasaba moraine dam based on the heat transfer module of COMSOL Multiphysics. The results show that the soil temperature of the moraine dam can be adequately simulated using the COMSOL Multiphysics heat transfer module and the simulated temperature values are generally consistent with the observed trends, yielding root mean square errors (RMSEs) less than 1.58 ℃ and Nash-Sutcliffe efficiency coefficients (NSEs) between 0.66 and 0.93. The average annual increase of the active layer depth was 0.026 m/a from 1959 to 2020. The buried ice inside the moraine dam was evidently melting and the maximum buried ice thawing depth under scenarios SSP1-2.6, SSP2-4.5, and SSP5-8.5 in CMIP6 (Coupled Model Intercomparison Project Phase 6) is expected to be 11.3 m, 18.4 m, and 23.5 m, respectively, by the end of the century, which indicates a continuous deterioration of the moraine dam stability.

Plain Language Summary

Glacial Lake Outburst Floodings (GLOFs) in the Tibetan Plateau have been frequent in recent years, which caused a large number of casualties and property damage. In this research, we paid more attention to the stability of moraine dams and simulated freeze/thaw and buried ice melting process of Longbasaba moraine dam from 1959 to 2100 using the heat transfer module of COMSOL Multiphysics. In the past decades, the active layer thickness was increasing and the buried ice began to melt since the early 1980s. Under the future warming scenarios, the dam melting depth will be greater than the freezing depth, and the rate of buried ice melting inside the dam will accelerate. This phenomenon indicates that the seepage/pipe will increase and the stability of the moraine dam has been continuously deteriorating. In the future, we must be alert to the possibility of dam failure disasters.

1 Introduction

The lower elevation limit for permafrost on the northern slopes of the Himalayas is considered to be 5100–5300 m above sea level (a.s.l.) (Gruber, 2012; Zou et al., 2017), yet thousands of moraine-dammed lakes exist above this limit (Nie et al., 2013; Otto, 2019; Wang et al., 2021; Zheng et al., 2021). These moraine dams are mainly composed of poorly sorted sediments, permafrost, and buried ice (Iribarren Anacona et al., 2015; Westoby et al., 2014; Worni et al., 2012). In the context of climate warming, the water pressure to moraine dams has increased in recent decades owing to rapid glacial retreat and glacial meltwater accumulation in lake basins (Che et al., 2021; Daiyrov et al., 2018; Gardelle et al., 2011; Li et al., 2021; Yao et al., 2010). Climate warming also affects the internal structure of moraine lake dams and consequently their stability (Bolch et al., 2011; Neupane et al., 2019). Buried ice is one of the most important factors for assessing the stability and susceptibility of moraine dams to failure (Emmer&Vilímek, 2013; Falatkova et al., 2019; Rounce et al., 2016; Worni et al., 2012), and the distribution and changes of buried ice are directly related to the temperature field inside the dam (Daiyrov et al., 2018; Falatkova et al., 2019; Wang et al., 2022). Upon melting of buried ice inside a moraine dam, the dam surface will sink and interior cavities will expand, thus possibly reducing the water-resistance stress and increasing the dam instability (Emmer&Cochachin, 2013; Kenner, 2019). Analysis of the relationship between the temperature field and internal structural changes of moraine dams is of theoretical significance and practical application value to better understand and mitigate glacial lake outburst floods.

Moraine dam failure can be triggered by the degradation of ice-cored moraine and permafrost owing to rising temperatures, increasing hydrostatic pressure due to lake expansion, and tsunami-like waves from a detached mass (e.g., ice, rock, landslide) from creeping lake sidewalls (Byers et al., 2019; Westoby et al., 2014; Worni et al., 2012). The dynamics of moraine-dammed lake basins has therefore been extensively monitored. Interferometric synthetic aperture radar (INSAR) and persistent scatterer interferometry (Dini et al., 2019; Hooper et al., 2012; Li et al., 2015; Tofani et al., 2013) techniques have been used to investigate the stability of moraines and slopes around glacial lakes. Ground-penetrating radar, electrical resistivity tomography, and the self-potential method (Harrison et al., 2022; Rajaure et al., 2018; Thompson et al., 2012) have been used to detect the internal structure and seepage state inside moraine dams. Most existing studies on moraine dam stability involved a qualitative analysis of the geometrical shape, surface morphology, internal structure, and seepage conditions of a moraine dam. Later studies addressed the moraine dam failure mechanisms, shifting from experimental investigations (Balmforth et al., 2008; Balmforth et al., 2009) to numerical solutions (Begam et al., 2018; Hubbard et al., 2005; McKillop&Clague, 2007; Minussi&Maciel, 2012; Osti et al., 2011). Moraine dam research has thus transitioned from qualitative descriptions of moraine dam morphology and internal dam structures to quantitative analysis using a combination of field observations and simulation tests.

Simulating the variations of hydrothermal regimes within a dam is fundamental to further assess dam stability (Saito et al., 2007; Wang et al., 2018). In permafrost areas, the ability of moraine dams with similar geometric shapes and internal structures to resist hydrostatic pressure and seepage- or piping-induced dam failure may differ owing to changing hydrothermal status (Haeberli et al., 2017a; Wang et al., 2012). Numerical methods can be used to simulate the freeze-thaw process of permafrost (Wei et al., 2021; Zhao et al., 2016), predict future permafrost distribution trends (Malevsky-Malevich et al., 2001; Nan et al., 2005; Ni et al., 2021a; Wu et al., 2018), and estimate active layer thicknesses (Pang et al., 2011; Qin et al., 2017; Wu et al., 2012). Many statistical-empirical models (Li&Cheng, 1999; Zhang et al., 2008) and numerical models (Harlan, 1973; Riseborough et al., 2008; Taylor&Luthin, 1978) related to temperature have been proposed on frozen soil or artificial earth and rock dams (Su et al., 2009; Wang et al., 2011), yet relatively few studies have numerically modeled the temperature of moraine dams in high-cold mountain areas. COMSOL Multiphysics has been reported to present certain advantages in solving multiphysics field coupling problems, and is widely used to simulate perennial permafrost heat conduction problems that contain phase changes (Huang et al., 2022; Noetzli et al., 2007; Yan et al., 2020; Zhang et al., 2018). However, few studies have used COMSOL Multiphysics to simulate moraine dams.

In this paper, we simulated the soil temperature field of the Longbasaba moraine dam from 1959 to 2021 based on the heat transfer module of COMSOL Multiphysics using the daily average air temperature and hydrothermal parameters. We also simulated the melting process of buried ice in in the moraine dam under scenarios SSP1-2.6, SSP2-4.5, and SSP5-8.5 of CMIP6 (Commentary on the Coupled Model Intercomparison Project Phase 6) to estimate the effects of freeze-thaw processes during this century.

2 Study Area

The moraine-dammed Longbasaba Lake (27°57′N, 88°04′E; 5520 m a.s.l.) is located at the source of the Pumqu River watershed in the northern Himalayas (Figure 1a) and is reported to face a very high probability of dam failure (Wang et al., 2012; Wang et al., 2008). The annual average air temperature is −3.6 °C and the average humidity is 40% (Wang et al., 2018). The maximum water depth in 2009 was 101.9 m with an average depth of 47.5 m and total water volume of $6.4\times10^7 m^3$ (Yao et al., 2012). The Longbasaba glacier is connected to Longbasaba Lake (Figure 1b), and a debris-covered glacier with ice cracks and serac pillars extends into the lake (Figure 1d). The moraine dam is mainly composed of coarse-grained granite with ice cores, has an average top width and length of 163 and 388 m, respectively, and is 100 m high from bottom to top (Wang et al., 2008). Several small ponds have developed in depressions of the dam (Figure 1e). Buried ice covered by approximately 1–3 m of debris is exposed in the central part of the inner flank of the moraine dam (Figure 1f) (Wang et al, 2018).

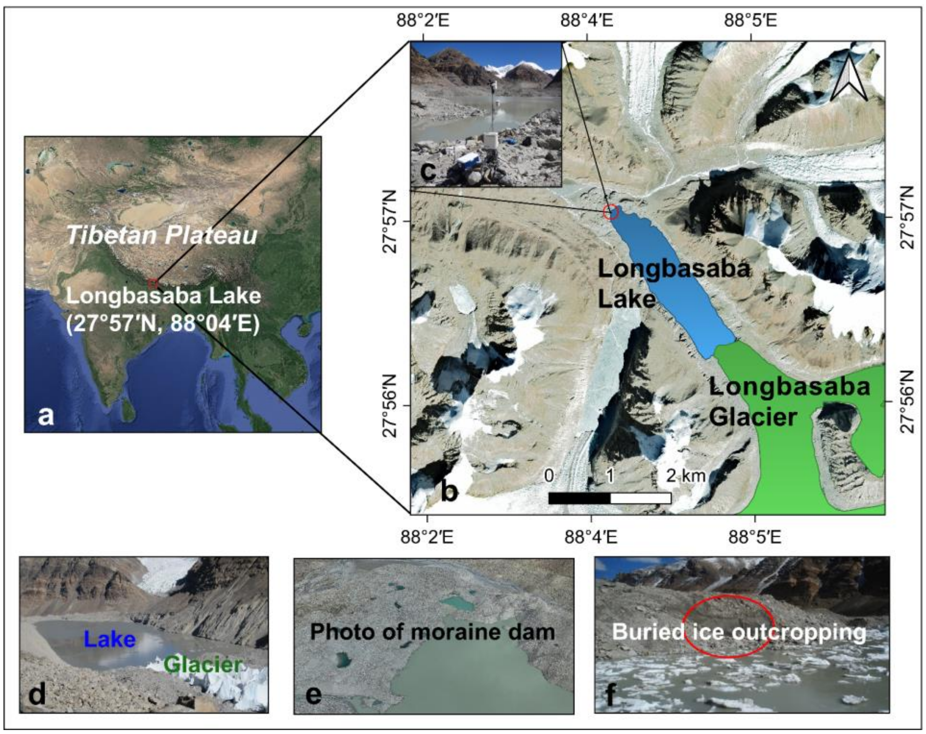

Figure 1. (a) Location map of Longbasaba Lake. (b) Longbasaba Lake and Longbasaba glacier (Google Earth image in December 2020). (c) Observation site and automatic meteorological station on the moraine dam at Longbasaba Lake (photograph taken in August 2012). (d) Photograph of Longbasaba Lake (photograph taken in October 2009). (e) Photograph of moraine dam filmed by an unmanned aerial vehicle in September 2021. (f) Exposed buried ice inside dam (photograph taken in August 2012).

3 Data

The data used in this paper mainly include air temperature data (air temperature on the dam and from the Dingri meteorological station station, and future air temperature of CMIP6), soil temperature, moisture content inside the moraine dam, and deformation data on the dam surface (Table 1).

Table 1
Description of Data Used in this Study.

Data Type	Accuracy	Description	Time period
Air/soil temperature data on the dam	~±0.2 °C	Temperature Probes recorded by Campbell CR3000-XT	November 2012-September 2021
Soil moisture content of dam	±2.5%	Water Content Reflectometer recorded by Campbell CR3000-XT	November 2012-Septemper 2021
Daily air temperature	~±0.1°C	From Dingri meteorological station	January 1959-March 2021
Future air temperature scenarios	~±0.1°C	From CMIP6 Official Website	January 2015-December 2099
Dam surface deformation	~±0.001 mm	Obtained by PS-INSAR	March 2017-October 2020

An automatic meteorological station was installed in 2012 to record the air temperature, soil moisture probes, ground heat flux, soil temperature, and other variables on the moraine dam (Figure 1c). All of the sensors were connected to a data logger (Campbell CR3000-XT) for automatic recording every 10 min. The daily average air temperature was collected from the Dingri meteorological station (28°38′N, 87°05′E, 4300 m a.s.l.) in 1959–2021. A linear regression model (soil temperature = 0.7794 × air temperature − 1.925, $R^2 = 0.8705$, $\alpha < 0.001$) was established to reconstruct the surface temperature of the moraine dam during the period 1959–2012 based on daily mean air temperature data from the Dingri meteorological station and daily mean soil temperature data at 10 cm depth in the moraine dam from 2012 to 2021 (Figure 2a). According to this equation, the daily mean soil temperature at 10 cm depth in the moraine dam was extended backward using daily mean air temperature data from the Dingri station for the period 1959–2012 (Figure 2b).

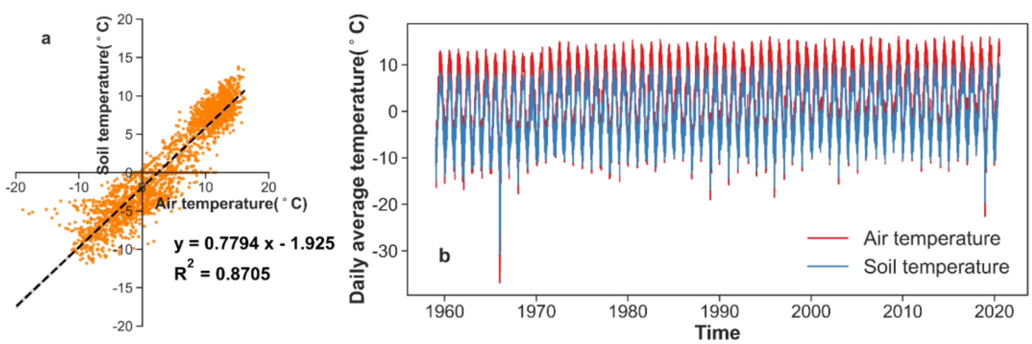

Figure 2. (a) Relationship between daily mean air temperature from the Dingri meteorological station and the daily mean soil temperature at 10 cm depth in the Longbasaba Lake moraine dam during the period of 2012–2021. (b) Variations of air temperature from the Dingri meteorological station and the reconstructed soil temperature at 10 cm depth in the Longbasaba Lake moraine dam, shown by the daily mean temperature in 1959–2021.

Future scenario daily average near-surface air temperatures for SSP1-2.6, SSP2-4.5, and SSP5-8.5 in 2015–2099 were taken from the CMIP6 official website. Eight climate models with good air temperature–soil temperature correlations ($R^2 > 0.5$) were selected based on air temperature and soil temperatures from 2015 to 2021. The resolutions of the climate models with their soil–air temperature linear regression expressions and correlation coefficients (R^2) are listed in Table 2.

Table 2

Climate Models Used in this Study.

Source ID	Nominal Resolution	Soil –air temperature linear regression expression	R^2
ACCESS-ESM1-5	250 km	y = 0.9779x - 21.755	0.6316
BCC-CSM2-MR	100 km	y = 0.9676x - 21.536	0.7129
CanESM5	500 km	y = 0.8798x - 19.901	0.7268
CNRM-ESM2-1	250 km	y = 0.8801x - 18.251	0.7024
CAMS-CSM1-0	100 km	y = 0.6437x + 18.763	0.6896
EC-Earth3-Veg	100 km	y = 0.9704x - 21.481	0.5894
IPSL-CM6A-LR	250 km	y = 0.9764x - 21.627	0.5593
MIROC6	250 km	y = 1.1575x - 23.154	0.5184

According to expressions in Table 2, the daily mean soil temperature at 10 cm depth in the moraine dam was extended forward using daily mean air temperature data from the CMIP6 official website for the period 2015–2099. The trend of the annual mean surface and 10 cm soil temperatures under the future scenarios of SSP1-2.6, SSP2-4.5, and SSP5-8.5 are shown in Figure 3.

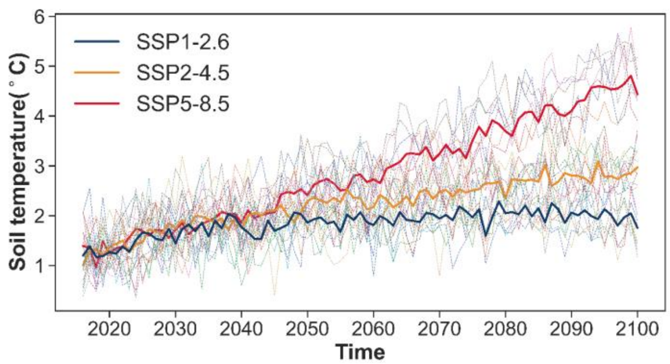

Figure 3. Annual mean 10 cm soil temperature changes of the dam surface in future scenarios. Solid lines indicate the average temperature for all climate models; dashed lines are the temperatures for each model.

We also used interferometric PS-INSAR to monitor the dam surface deformation. The data sources included 44 views of Sentinel-1A from 2017 to 2020 ascending orbit images processed by Gamma. The data source is shown in Table 3.

Table 3

Data source of the Sentinel-1A Ascending Orbit Images.

Image Parameters	Values
Sensor	S1A IW IW1 VV
Date range	2017/03/12-2020/10/10
Temporal resolution	12 days
Center latitude	27.69°N
Center longitude	88.42°E
State vector interval	10 s
Incidence angle	33.97°

4 Methodology

4.1 Model Description

Numerical simulations of the soil temperature variation and freeze-thaw process in the Longbasaba moraine dam were carried out using COMSOL Multiphysics 5.6 software based on a one-dimensional transient solid heat transfer interface in the heat transfer module (Figure 4). The calculated depth in this model was set to 50.0 m, with reference to the average thickness near the terminal section of the Longbasaba glacier (40.2–75.8 m) (He et al., 2021) and the height of the Longbasaba moraine dam (~100 m) (Wang et al., 2008). The material below 2.5 m was set as a mixture of gravel and buried ice to simulate the melting of buried ice inside the dam. The time step of the model calculation was 1 day, and the calculation grid cell was 1 cm (Figure 4). The basic inputs for the modeling procedure included the heat conduction equation, boundary and initial conditions, and soil hydrothermal parameters.

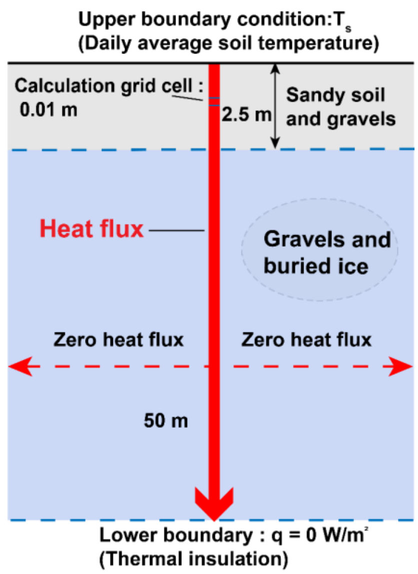

Figure 4. Sketch map of the numerical model of one-dimensional heat transfer.

COMSOL Multiphysics model was used in this paper, and the operations in the development of the heat transfer equation were simplified as follows: (1) when the soil is layered, the soil skeleton has no expansion or contraction deformation, and each layer is uniformly continuous and isotropic (Nixon&McRoberts, 1973); (2) the temperature distribution is smooth and continuous in both time and space (Harlan, 1973); (3) free thermal convection in frozen soil is negligible (Kane et al., 2001); (4) hydrothermal parameter changes are not considered owing to solute migration (Saito et al., 2007); and (5) when the soil is completely frozen, the unfrozen water is assumed to be a definite value (Harlan, 1973; Nixon&McRoberts, 1973)；(6) when the buried ice melted into water in certain depth, of which the parameters of material is filled by soil's due to the water flowing away.

4.2 Model Set-up

4.2.1 Heat Conduction Equation

The heat transfer model of COMSOL Multiphysics is based on analysis of coupled heat–fluid transport in partially frozen soil (Harlan, 1973; Riseborough, 2004). The heat conduction of the soil medium and in situ phase change of ice and water were taken into account in the model, in which the latent heat of the phase change is regarded as the internal heat source (Tan et al., 2011). Owing to the low overall water content (4%) (Table 4), the effect of moisture convection heat transfer is ignored for the simplification of the model and can be regarded as solid heat transfer

(Taylor&Luthin, 1978). The one-dimensional transient heat transfer differential equation based on the heat transfer module of COMSOL Multiphysics was established as:

$$\rho C \frac{\partial T}{\partial t} = \frac{\partial}{\partial z}\lambda \frac{\partial T}{\partial z} + L\theta_i \qquad (1)$$

where ρ, λ, and C are the density, thermal conductivity, and heat capacity of the soil medium, respectively, T is the soil temperature, t is the time, z is the downward vertical coordinate, L is the mass specific latent heat of fusion for the water phase change (at 0 °C L = 333.7 kJ · kg^{-1} and θ_i is the rate of liquid water and ice content change induced by freezing or thawing. The effects of the air phase and radiation are neglected because the phase transition of water predominates in the process of energy conversion.

4.2.2 Boundary and Initial Conditions

The boundary and initial conditions are collectively referred to as the margin conditions. Boundary conditions indicate the mutual heat transfer between the soil and surrounding medium at the geometric boundary (Zhang et al., 2019). The upper boundary condition is a Dirichlet boundary condition, T_s for the daily mean near-surface 10 cm soil temperature time series. The climate time series CMIP6 scenario can also be integrated to simulate future scenarios. The lower boundary condition was set as a Neumann boundary condition with a heat flux (q). Heat exchange at the bottom of the dam was neglected, q = 0 W/m^2 (thermal insulation) (Figure 4).

The initial conditions indicate the temperature distribution of the soil at the instant the process begins (Riseborough et al., 2008). To obtain the initial temperature condition (T_0), the temperature of the starting year was cyclically calculated for 1000 a, and when the temperature (−1.66 °C) at the lower part of the dam stabilized, it was selected as the T_0 value of this model (Figure 5).

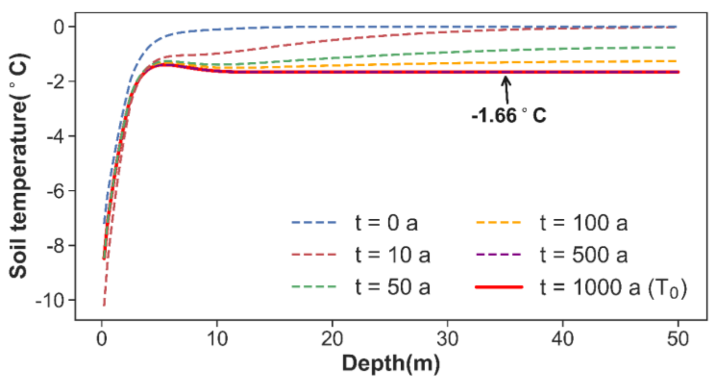

Figure 5. Initial temperature field of this model.

4.2.3 Hydrothermal Parameters

The Longbasaba Lake moraine dam is mainly composed of sandy soil and gravels with little difference in terms of material composition at depths from 0–2.5 m in summer with buried ice existing below 2.5 m depth, as indicated by a manually excavated profile (Wang et al., 2008). The hydrothermal state of the ground heat flux, temperature, and moisture content inside the moraine dam presented evident stratification at different depths of 0–0.5, 0.5–2.5, and below 2.5 m in the dam (Wang et al., 2018).

The thermal conductivity (λ) of freeze-thaw soil is closely related to the material composition of the soil and can be calculated according to the thermal conductivity of the constituent substances and their corresponding volume ratios following:

$$\lambda_u = {\lambda_s}^{\phi 1} {\lambda_a}^{\phi 2} {\lambda_w}^{\phi 3} \quad (2)$$

$$\lambda_f = {\lambda_s}^{\phi 1} {\lambda_a}^{\phi 2} {\lambda_i}^{\phi 3} \quad (3)$$

where λ_u and λ_f are the thermal conductivity of the molten soil and frozen soil, respectively, λ_s, λ_a, λ_w, and λ_i are the thermal conductivity of soil, air, water, and ice, respectively, and $\phi 1$–$\phi 3$ are the volume ratios of the corresponding constituents.

The volumetric heat capacity of the soil is calculated as:

$$C_u = C_{du} \rho_u \quad (4)$$

$$C_f = C_{df} \rho_f \quad (5)$$

where C_u and C_f are the volumetric heat capacities of molten soil and frozen soil, respectively, C_{du} and C_{df} are the specific heats of molten soil and frozen soil, respectively, and ρ_u and ρ_f are the natural capacities (wet capacities) of molten soil and frozen soil, respectively (kg/m^3).

The main difference between frozen soil and thawed soils is the presence of ice. Experiments have shown that the specific heat of soil has the property of a weighted average by the mass of each material component (the content of gas-phase fillings in the soil and the specific heat are small and negligible), i.e.,

$$C_{du} = \frac{C_{su} + W C_w}{1+W} \quad (6)$$

$$C_{df} = \frac{C_{sf} + (W - W_u) C_i + W C_w}{1+W} \quad (7)$$

where C_{su}, C_{sf}, C_w, and C_i are the specific heat values of the melt skeleton, frozen soil skeleton, water, and ice, respectively. As a rule, C_w=4.128 kJ/(kg·°C), W is the water content, and W_u is the unfrozen water content.

To determine the physical properties of the ground material, optimization-based inverse techniques are applied to fit the simulated temperatures to the measured ones (Nicolsky et al., 2009). The Levenberg-Marquardt algorithm as implemented in the optimization module relies on two fundamental ideas: evaluation of an approximate Hessian and regularization of the Hessian approximation. The special structure of least-squares objective functions allows cheap evaluation of an approximate Hessian (matrix of second derivatives), which can in principle be used directly in a Newton iteration. The objective function is:

$$V(\eta) = \frac{1}{2} \sum_{m=1}^{M} \sum_{j=1}^{J_m} \sum_{k=1}^{K_{jm}} \omega_{jm} f_{jm}^2 \left(x_{jmk} u_m \left(x, p_{jm}, \eta \right), \eta, C_m \right) \quad (8)$$

where M is the number of series (measurement series), J_m is the number of measurements, K_{jm} is the number of points, the variable x is the space coordinates, η are the parameters for which the cost function should be minimized, and u_m (x,p,η) solves a given partial differential equation or ordinary differential equation, which refers to the heat conduction equation (1) in this study. The optimization tolerance was set as 0.01. Soil thermophysical properties of each layer were determined according to the reference value of national standard GB50324-2001 (2014) and model optimization. The parameters after Levenberg-Marquardt optimization are listed in Table 4.

Table 4

Soil Parameter Results after Optimization.

<table>
<tr><th rowspan="2">Depth (m)</th><th colspan="2">Density, ρ (kg/m^3)</th><th rowspan="2">Volumetric water content (%)</th><th colspan="3">Thermal conductivity, λ W/(m·K)</th><th colspan="3">Volumetric heat capacity, C kJ/(m^3·K)</th></tr>
<tr><th>ρ_s</th><th>ρ_i</th><th>λ_u</th><th>λ_f</th><th>λ_i</th><th>C_u</th><th>C_f</th><th>C_i</th></tr>
<tr><td>0-0.5</td><td rowspan="3">1706</td><td rowspan="2">-</td><td rowspan="2">3.95</td><td>0.52</td><td>1.11</td><td>–</td><td>1463.7</td><td>1200.2</td><td>–</td></tr>
<tr><td>0.5-2.5</td><td>0.65</td><td>1.52</td><td>–</td><td>1697.9</td><td>1317.3</td><td>–</td></tr>
<tr><td>>2.5</td><td>920</td><td>-</td><td>0.78</td><td>–</td><td>2.18</td><td>1568.3</td><td>–</td><td>2100</td></tr>
</table>

Note: Subscripted u and f denote the unfrozen and frozen states of the soil, while s and i denote the material of the soil and ice, respectively.

5 Results

5.1 Model Verification

In this study, the root mean square error (RMSE), and Nash-Sutcliffe efficiency coefficient (NSE) were used to evaluate the simulation accuracy (Wei et al., 2021; Zhao et al., 2016). The equations for the RMSE and NSE are as follows:

$$RMSE = \sqrt{\frac{\sum_{i=1}^{N}(s_i - o_i)^2}{N}} \tag{9}$$

$$NSE = 1 - \frac{\sum_{i=1}^{N}(s_i - o_i)^2}{\sum_{i=1}^{N}(s_i - \bar{o})^2} \tag{10}$$

where s_i and o_i are the simulated and observed values of the i^{th} sample, respectively, $\bar{o}$ is the mean of the observed value, and N is the number of samples. The RMSE emphasizes the variation of an error within an individual station, and the NSE reflects the degree of agreement between the simulated and observed values with time.

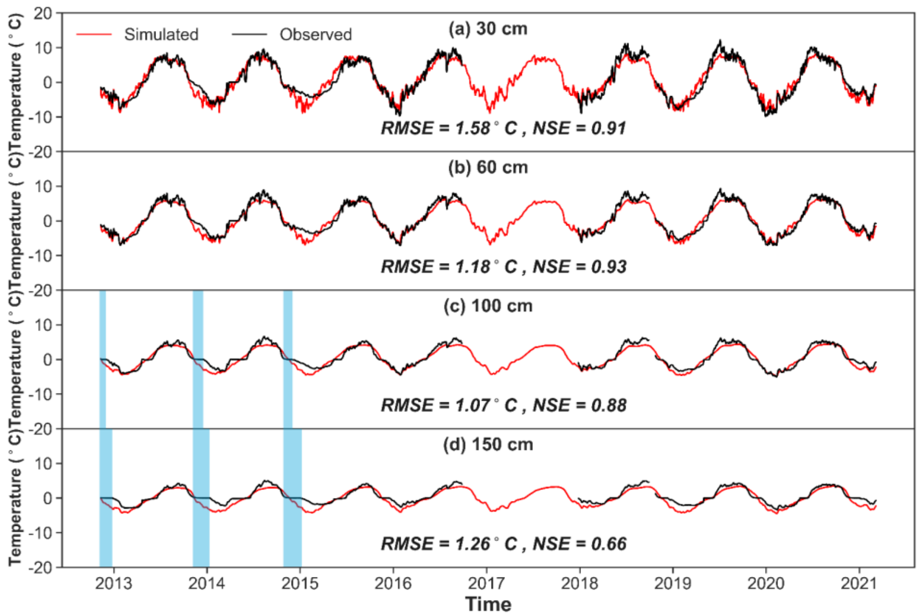

Figure 6. Comparison of the soil temperature simulation results at depths of 30 cm (a), 60 cm (b), 100 cm (c), and 150 cm (d) (Observation data are missing for 2016/9/24–2017/12/3 and 2018/9/29–2018/10/2 owing to capacity limitations of the data acquisition equipment). The observed zero-curtain periods were marked by light blue in (c) and (d).

The results show that the RMSEs of the simulated and observed soil temperatures at 30, 60, 100, and 150 cm depth are 1.58 °C, 1.18 °C, 1.07 °C, and 1.26 °C, respectively, and the NSEs of are 0.91, 0.93, 0.88, and 0.26 (Figure 6). The average RMSE of the four layers is 1.27 °C and the NSE layers vary from 0.66 to 0.93, which indicates a reasonable model simulation result.

5.2 Simulation of Dam Freeze-Thaw Process

The freeze-thaw cycle curves simulated by the heat transfer module of COMSOL Multiphysics showed that the thawing and freezing fronts intersected in early March to early April. From 1959 to 2020, the change of the active layer thickness (ALT) varied by 1.8–3.6 m, reaching a maximum of 3.6 m in 2019, and exhibited an overall increasing trend with an average annual thawing rate of 0.026 m/a, even though the active layer thickness decreased over a short period from the mid-1960s to 1970 (Figure 7).

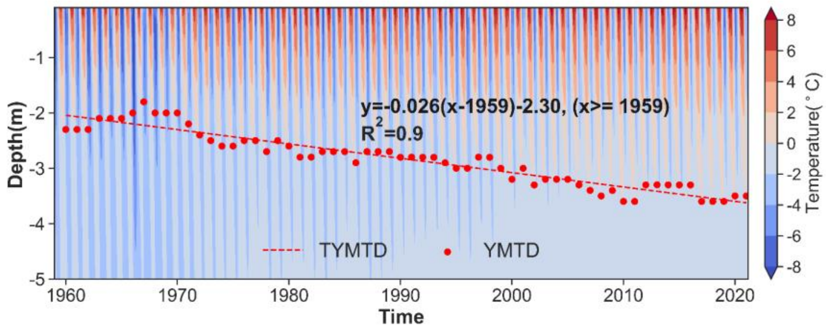

Figure 7. Change of the active layer from 1959 to 2020 (YMTD, yearly maximum thawing depth; TYMTD, trend of yearly maximum thawing depth).

In the future scenarios, a thawed layer developed in winter starting in ~2065 as the seasonal thaw depth in summer, which was permanently larger than the freeze depth in winter under scenario SSP1-2.6 (Figure 8a), and a permanent thawed layer shift appeared in ~2055 inside the moraine dam in scenarios SSP2-4.5 and SSP5-8.5 (Figure 8b, c). Thus henceforward, the moraine dam developed into an upper seasonal freeze-thaw layer, a middle permanently thawed layer, and a lower permafrost/ice layer. The seasonal freezing depth became increasingly shallow with hardly any cycle freeze-thaw processes occurred later in the century under scenario SSP5-8.5.

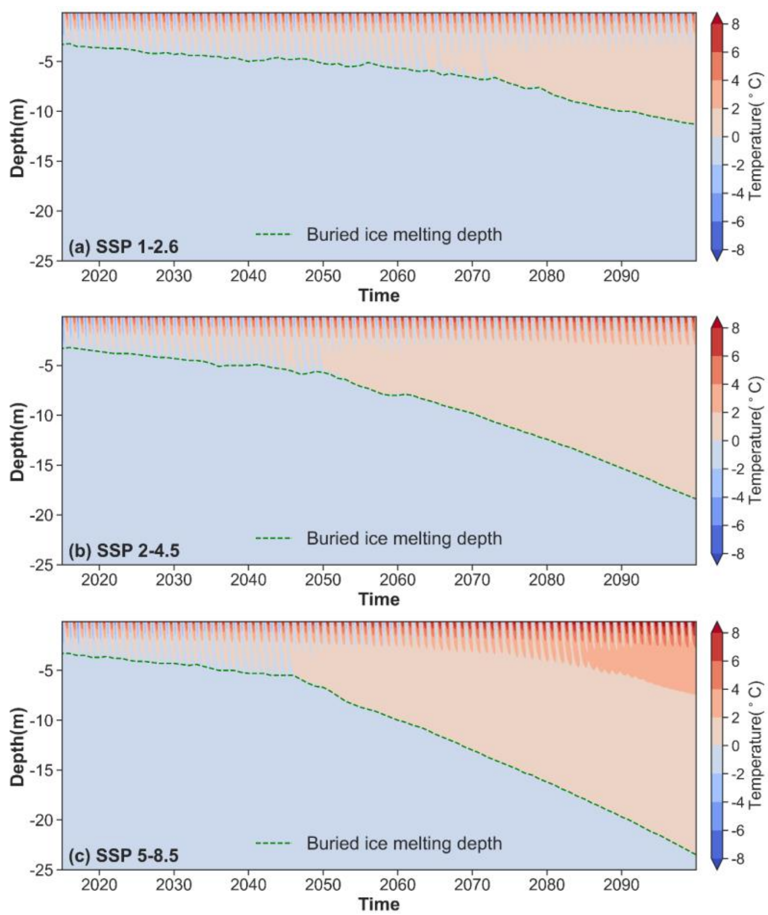

Figure 8. Freeze-thaw process of Longbasaba Lake moraine dam under future scenarios SSP1-2.6 (a), SSP2-4.5 (b), and SSP5-8.5 (c) during this century. The dashed zero isotherm line indicates the melting depth of the buried ice.

5.3 Estimation of Buried Ice Melting Scenarios

Buried ice melting occurs when the summer melt depth and thawing front increase in summer. The buried ice began to melt in ~1980 when the maximum thawing front in summer reached ~2.5 m depth. The maximum melting depth has since deepened, reaching 3.5 m in 2020. In scenarios SSP1-2.6, SSP2-4.5, and SSP5-8.5, the maximum melting depth of the buried ice is expected to occur at average depths of 11.3, 18.4, and 23.5 m, respectively, indicating zero isotherm deepening inside the dam by the end of this century (Figure 8). The melting rates of buried ice are 0.05–0.09 m/a with no significant difference among the SSP1-2.6, SSP2-4.5, and SSP5-8.5 scenarios before the year 2050, while the melting rates accelerated to 0.14 to 0.33 m/a in the different scenarios during the second half of the 21st century.

6 Discussion

6.1 Uncertainties and Limitations

Although the simulated and observed values are relatively similar, there remain some uncertainties in this model. For example, the lower boundary geothermal heat flow conditions of the dam are unknown owing to limitations of the observation conditions. These may be thermally insulated conditions or there may be fluxes that affect the overall results to some degree (Hu, 1992; Qin et al., 2017). In this paper, the bottom boundary conditions are assumed to be thermally insulated because (1) the dam is constituted by a secondary, covered moraine on the valley bed and (2) large, buried ice inside the moraine dam may be naturally thermally insulated material that keeps the geothermal heat flowing upward. The heat change caused by moisture migration was usually mutable and elusory in the loose moraine (Kane et al., 2001; Taylor&Luthin, 1978) and can be ignored when the observed soil moisture content is low (Zhao et al., 2008). This model does not consider convective heat transfer above 2.5 m depth because it was characterized by a low value (average ~4%) in the moraine dam of Longbasaba Lake compared with other frozen soil of the Tibetan Plateau (Wang et al., 2018).

The errors between the simulated and observed values also show seasonal differences, characterized by smaller values in summer and relatively larger values in winter. This may possibly be related to presence of significant snow cover on the dam in winter, which reduces the correlation between the ground and air temperatures owing to its insulating effects (Haeberli et al., 2017b; Staub&Delaloye, 2017). The average water content value of each layer set in this model is also not a good solution for the error caused by latent heat when the soil undergoes a phase change, owing to large soil water content fluctuations with seasonal changes. For example, in 2013–2015 at 1.0 m and 1.5 m, the observed three zero-curtain periods occurred during late October to early February of the following year, whereas the simulated soil temperature varied by -0.13 to -3.27 °C over the same time interval. This indicates that the simulation failed to capture this change process owing to insufficient consideration of latent heat (Figure 6c, d).

The upper boundary conditions of this model depend on the temporal and spatial correlation of the soil and air temperatures at appropriate scales. The output was reduced using a regional-scale atmospheric model, and a stepwise multiple regression was then performed to create an equation that best fits the predictions to site-specific observations using the bilinear interpolation output of the atmospheric model (Zhang et al., 2012). This approach bridges the scale difference between atmospheric climate models and permafrost thermal models, and allows a wider range of factors to be used for predicting thermal boundary conditions. By constructing such an atmosphere–permafrost model, it can then be used to predict changes in boundary condition parameters under different future greenhouse gas emission scenarios (e.g., CMIP6).

6.2 Deteriorating Stability of the Moraine Dam

Climate-induced changes in the permafrost environment have recently been reported to be widespread and accelerating in the Tibetan Plateau (Jin et al., 2021; Liu et al., 2022; Ni et al., 2021b). The simulation results indicate that the ALT presented an annually increasing trend from 1959 to 2020 in the moraine dam of Longbasaba Lake (Figure 7), showing an intensified permafrost degradation trend of the moraine dam since the 1980s in response to rising air temperature. A permanent thaw layer inside the dam developed that was deemed likely to progress into dam seepage after the year 2055–2065, and would gradually thicken under scenarios SSP2-4.5 and SSP5-8.5 in this century. With the increasing maximum thawing depth of the Longbasaba Lake moraine dam, the capacity for water blocking and anti-piping of the moraine dam would decrease, while the outflow would increase as the thawed moraine becomes more prone to erosion than the frozen moraine, which would reduce the dam body stability (Wang et al., 2008; 2018). For example, the outlet shape of Longbasaba Lake in 2006 was ~2 m wide and ~1 m deep. This expanded to ~5 m wide and ~3 m deep in 2020, as indicated by a rough in situ survey (Figure 9).

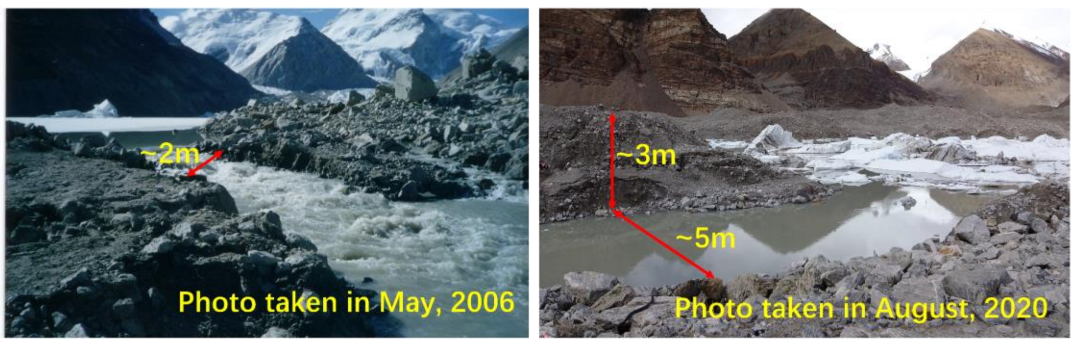

Figure 9. Outlet of the Longbasaba Lake moraine dam was evidently expanding.

Buried ice in the dam has melted, as evidenced by the deepening of the thaw front in summer, to reach or even exceed the depth of buried ice in recent decades. This process is predicted to accelerate in the future, resulting from the annual positive surplus of heat reaching the inner moraine dam (Wang et al., 2018). As buried ice melts, the thermal-karst development and viscous flow would likely increase in the moraine dam and the probability of the dam's failure would increase. On the other hand, the buried ice melting and permafrost thaw would likely produce considerable thaw settlement and surface subsidence at sites with ice-supersaturated materials inside the moraine dam. The Longbasaba moraine dam caved in with a maximum sinking rate of 0.15 m/a from 2017 to 2020 according to interferometric PS-INSAR monitoring (Figure 10). It can be inferred that there existed an intrinsic link between dam sinking and buried ice melting (Astakhov et al., 1996). If the maximum rate is maintained, the average water depth may decrease. Such surface subsidence related to buried ice melting in the moraine dam may affect lake water levels and consequently the ability to hold melting water from the Longbasaba glacier.

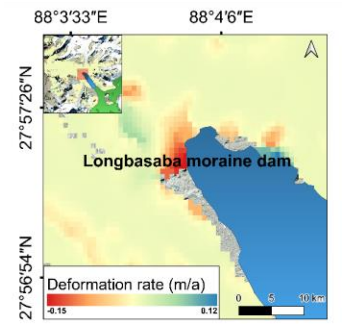

Figure 10. Deformation detection of the Longbasaba moraine dam (positive values represent uplift, negative values represent subsidence).

7 Conclusions

Simulations were conducted on the freeze-thaw process of a moraine dam of Longbasaba Lake using COMSOL Multiphysics software and multi-source data, and the melting rate of interior buried ice was estimated. The soil temperature field of the moraine dam is well simulated using the COMSOL Multiphysics heat transfer module with errors vary from 1.07 °C to 1.58 °C, with an average root mean square error of 1.27 °C compared with observed soil temperatures of different layers. The ALT increased from 1959 to 2020, with an average annual thawing rate of 0.026 m/a. The melting of buried ice in the dam has evidently occurred since 1980 and is expected to accelerate in the future. A thawed layer began to develop in winter since the year of 2055-2065 as seasonal thaw depth in summer was permanently larger than the freeze depth in winter. The maximum melting depths of the buried ice are expected to be 11.3 m, 18.4 m and 23.5 m by the end of this century in scenarios SSP1-2.6, SSP2-4.5, and SSP5-8.5, respectively. An increase of the maximum thawing depth and acceleration of buried ice melting in the Longbasaba Lake moraine dam will reduce the capacity of the dam for water blocking and reduce anti-piping and erosion prevention, which will consequently further destabilize the dam body.

Acknowledgments

The authors would like to thank Guangli He and Te Zhang for their field support. We also thank Esther Posner, PhD, from Liwen Bianji (Edanz) (www.liwenbianji.cn) for editing the language of a draft of this manuscript. This study was supported financially by the National Natural Science Foundation of China [grant No. 42171137, 42171134, 41771075].

Author Contributions

Conceptualization: Xin Wang, Yanlin Zhang, Jia Wang
Data curation: Jia Wang, Xin Wang, Weijie Ran, Qiao Liu
Formal analysis: Jia Wang, Xin Wang, Yanlin Zhang, Weijie Ran
Funding acquisition: Xin Wang
Investigation: Jia Wang, Xin Wang, Yanlin Zhang
Methodology: Jia Wang, Xin Wang, Yanlin Zhang, Junfeng Wei, Yong Zhang, Qiao Liu, Dongyu Lei
Project Administration: Xin Wang
Resources: Xin Wang

Software: Jia Wang
Supervision: Xin Wang, Yanlin Zhang
Validation: Jia Wang
Visualization: Jia Wang
Writing – original draft: Jia Wang
Writing – review & editing: Xin Wang

Declaration of competing interest

The authors have no conflicts of interest to declare.

Data Availability Statement

The daily air temperature data (Dingri meteorological station) were obtained freely from the China Meteorological Administration (http://data.cma.cn/), and the future scenario air temperatures were taken from the CMIP6 official website (https://esgf-node.llnl.gov/search/cmip6).

References

Astakhov, V. I., Kaplyanskaya, F. A., &Tarnogradsky, V. D. (1996). Pleistocene permafrost of West Siberia as a deformable glacier bed, Permafrost and Periglacial Processes, 7(2), 165-191, https://doi:10.1002/(SICI)1099-1530(199604)7:23.0.CO;2-S.

Balmforth, N. J., von Hardenberg, J., Provenzale, A., &Zammett, R. (2008). Dam breaking by wave-induced erosional incision, Journal of Geophysical Research, 113(F1), https://doi:10.1029/2007jf000756.

Balmforth, N. J., Von Hardenberg, J., &Zammett, R. J. (2009). Dam-breaking seiches, Journal of Fluid Mechanics, 628, 1-21, https://doi:10.1017/s0022112009005825.

Begam, S., Sen, D., &Dey, S. (2018). Moraine dam breach and glacial lake outburst flood generation by physical and numerical models, Journal of Hydrology, 563, 694-710, https://doi:10.1016/j.jhydrol.2018.06.038.

Bolch, T., Peters, J., Yegorov, A., Pradhan, B., Buchroithner, M., &Blagoveshchensky, V. (2011). Identification of potentially dangerous glacial lakes in the northern Tien Shan, Natural Hazards, 59(3), 1691-1714, https://doi:10.1007/s11069-011-9860-2.

Byers, A. C., Rounce, D. R., Shugar, D. H., Lala, J. M., Byers, E. A., &Regmi, D. (2019). A rockfall-induced glacial lake outburst flood, Upper Barun Valley, Nepal, Landslides, 16(3), 533-549, https://doi:10.1007/s10346-018-1079-9.

Che, Y., Wang, S., Wei, Y., Pu, T., &Ma, X. (2021). Rapid changes to glaciers increased the outburst flood risk in Guangxieco Proglacial Lake in the Kangri Karpo Mountains, Southeast Qinghai-Tibetan Plateau, Natural Hazards, 110(3), 2163-2184, https://doi:10.1007/s11069-021-05029-5.

Daiyrov, M., Narama, C., Yamanokuchi, T., Tadono, T., Kääb, A., &Ukita, J. (2018). Regional Geomorphological Conditions Related to Recent Changes of Glacial Lakes in the Issyk-Kul Basin, Northern Tien Shan, Geosciences, 8(3), https://doi:10.3390/geosciences8030099.

Dini, B., Manconi, A., &Loew, S. (2019). Investigation of slope instabilities in NW Bhutan as derived from systematic DInSAR analyses, Engineering Geology, 259, https://doi:10.1016/j.enggeo.2019.04.008.

Emmer, A., &Cochachin, A. (2013). The causes and mechanisms of moraine-dammed lake failures in the Cordillera Blanca, North American Cordillera and Himalaya, Acta Universitatis Carolinae.geographica.univerzita Karlova, 48(2), 5-15, https://doi:10.14712/23361980.2014.23.

Emmer, A., &Vilímek, V. (2013). Review Article: Lake and breach hazard assessment for moraine-dammed lakes: an example from the Cordillera Blanca (Peru), Natural Hazards and Earth System Sciences, 13(6), 1551-1565, https://doi:10.5194/nhess-13-1551-2013.

Falatkova, K., Šobr, M., Neureiter, A., Schöner, W., Janský, B., Häusler, H., Engel, Z., &Beneš, V. (2019). Development of proglacial lakes and evaluation of related outburst susceptibility at the Adygine ice-debris complex, northern Tien Shan, Earth Surface Dynamics, 7(1), 301-320, https://doi:10.5194/esurf-7-301-2019.

Gardelle, J., Arnaud, Y., &Berthier, E. (2011). Contrasted evolution of glacial lakes along the Hindu Kush Himalaya mountain range between 1990 and 2009, Global and Planetary Change, 75(1-2), 47-55, https://doi:10.1016/j.gloplacha.2010.10.003.

Gruber, S. (2012). Derivation and analysis of a high-resolution estimate of global permafrost zonation, The Cryosphere, 6(1), 221-233, https://doi:10.5194/tc-6-221-2012.

Haeberli, W., Kääb, A., Mühll, D. V., &Teysseire, P. (2017a). Prevention of outburst floods from periglacial lakes at Grubengletscher, Valais, Swiss Alps, Journal of Glaciology, 47(156), 111-122, https://doi:10.3189/172756501781832575.

Haeberli, W., Schaub, Y., &Huggel, C. (2017b). Increasing risks related to landslides from degrading permafrost into new lakes in de-glaciating mountain ranges, Geomorphology, 293, 405-417, https://doi:10.1016/j.geomorph.2016.02.009.

Harlan, R. L. (1973). Analysis of coupled heat-fluid transport in partially frozen soil, Water Resources Research, 9(5), 1314-1323, https://doi:10.1029/WR009i005p01314.

Harrison, D., Ross, N., Russell, A. J., &Jones, S. J. (2022). Ground-penetrating radar (GPR) investigations of a large-scale buried ice-marginal landsystem, Skeiðarársandur, SE Iceland, Boreas, https://doi:10.1111/bor.12587.

He, G., Wei, J., &Wang, X. (2021). Thickness estimation of the Longbasaba Glacier: methods and application, Sciences in Cold and Arid Regions, 12(6), 477-490, https://doi:10.3724/SP.J.1226.2020.00477.

Hooper, A., Bekaert, D., Spaans, K., &Arıkan, M. (2012). Recent advances in SAR interferometry time series analysis for measuring crustal deformation, Tectonophysics, 514-517, 1-13, https://doi:10.1016/j.tecto.2011.10.013.

Hu, H. (1992). A numerical simulation for heat and moisture transfer during soil freezing, Journal of Hydraulic Engineering.

Huang, G., Guo, Y., Bescher, E., Gupta, R., &Liu, W. V. (2022). Numerical modeling of temperature profiles in hardening belitic calcium sulfoaluminate cement-based mortars for permafrost region applications, Journal of Sustainable Cement-Based Materials, 1-14.

Hubbard, B., Heald, A., Reynolds, J. M., Quincey, D., Richardson, S. D., Luyo, M. Z., Portilla, N. S., &Hambrey, M. J. (2005). Impact of a rock avalanche on a moraine-dammed proglacial lake: Laguna Safuna Alta, Cordillera Blanca, Peru, Earth Surface Processes and Landforms, 30(10), 1251-1264, https://doi:10.1002/esp.1198.

Iribarren Anacona, P., Mackintosh, A., &Norton, K. P. (2015). Hazardous processes and events from glacier and permafrost areas: lessons from the Chilean and Argentinean Andes, Earth Surface Processes and Landforms, 40(1), 2-21, https://doi:10.1002/esp.3524.

Jin, H.-J., Wu, Q.-B., &Romanovsky, V. E. (2021). Degrading permafrost and its impacts, Advances in Climate Change Research, 12(1), 1-5, https://doi:10.1016/j.accre.2021.01.007.

Kane, D. L., Hinkel, K. M., Goering, D. J., Hinzman, L. D., &Outcalt, S. I. (2001). Non-conductive heat transfer associated with frozen soils, Global and Planetary Change, 29(3-4), 275-292, https://doi:10.1016/s0921-8181(01)00095-9.

Kenner, R. (2019). Geomorphological analysis on the interaction of Alpine glaciers and rock glaciers since the Little Ice Age, Land Degradation & Development, 30(5), 580-591, https://doi:10.1002/ldr.3238.

Li, D., Shangguan, D., Wang, X., Ding, Y., Su, P., Liu, R., &Wang, M. (2021). Expansion and hazard risk assessment of glacial lake Jialong Co in the central Himalayas by using an unmanned surface vessel and remote sensing, Sci Total Environ, 784, 147249, https://doi:10.1016/j.scitotenv.2021.147249.

Li, X., &Cheng, G. (1999). A GIS-aided response model of high-altitude permafrost to global change, Science in China Series D: Earth Sciences, 42(1), 72-79, https://doi:10.1007/bf02878500.

Li, Z., Zhao, R., Hu, J., Wen, L., Feng, G., Zhang, Z., &Wang, Q. (2015). InSAR analysis of surface deformation over permafrost to estimate active layer thickness based on one-dimensional heat transfer model of soils, Sci Rep, 5, 15542, https://doi:10.1038/srep15542.

Liu, Q., Niu, J., Lu, P., Dong, F., Zhou, F., Meng, X., Xu, W., Li, S., &Hu, B. X. (2022). Interannual and seasonal variations of permafrost thaw depth on the Qinghai-Tibetan plateau: A comparative study using long short-term memory, convolutional neural networks, and random forest, Science of The Total Environment, https://doi:10.1016/j.scitotenv.2022.155886.

Malevsky-Malevich, S. P., Molkentin, E. K., Nadyozhina, E. D., &Shklyarevich, O. B. (2001). Numerical simulation of permafrost parameters distribution in Russia, Cold Regions Science and Technology, 32(1), 1-11, https://doi:10.1016/s0165-232x(01)00018-0.

McKillop, R. J., &Clague, J. J. (2007). Statistical, remote sensing-based approach for estimating the probability of catastrophic drainage from moraine-dammed lakes in southwestern British Columbia, Global and Planetary Change, 56(1-2), 153-171, https://doi:10.1016/j.gloplacha.2006.07.004.

Minussi, R. B., &Maciel, G. d. F. (2012). Numerical experimental comparison of dam break flows with non-Newtonian fluids, Journal of the Brazilian Society of Mechanical Sciences and Engineering, 34(2), 167-178, https://doi:10.1590/s1678-58782012000200008.

Nan, Z., Li, S., &Cheng, G. (2005). Prediction of permafrost distribution on the Qinghai-Tibet Plateau in the next 50 and 100 years, Science in China Series D: Earth Sciences, 48(6), 797-804, https://doi:10.1360/03yd0258.

Neupane, R., Chen, H., &Cao, C. (2019). Review of moraine dam failure mechanism, Geomatics, Natural Hazards and Risk, 10(1), 1948-1966, https://doi:10.1080/19475705.2019.1652210.

Ni, J., et al. (2021a). Simulation of the Present and Future Projection of Permafrost on the Qinghai-Tibet Plateau with Statistical and Machine Learning Models, Journal of Geophysical Research: Atmospheres, 126(2), https://doi:10.1029/2020jd033402.

Ni, J., et al. (2021b). Risk assessment of potential thaw settlement hazard in the permafrost regions of Qinghai-Tibet Plateau, Sci Total Environ, 776, 145855, https://doi:10.1016/j.scitotenv.2021.145855.

Nicolsky, D. J., Romanovsky, V. E., &Panteleev, G. G. (2009). Estimation of soil thermal properties using in-situ temperature measurements in the active layer and permafrost, Cold Regions Science and Technology, 55(1), 120-129, https://doi:10.1016/j.coldregions.2008.03.003.

Nie, Y., Liu, Q., Liu, S., &J-P., S. G. (2013). Glacial Lake Expansion in the Central Himalayas by Landsat Images, 1990–2010, Plos One, 8(12), e83973, https://doi:10.1371/journal.pone.0083973.

Nixon, J. F., &McRoberts, E. C. (1973). A Study of Some Factors Affecting the Thawing of Frozen Soils, Canadian Geotechnical Journal, 10(3), 439-452, https://doi:10.1139/t73-037.
Noetzli, J., Gruber, S., &Friedel, S. (2007). Modeling transient permafrost temperatures below steep Alpine topography.
Osti, R., Bhattarai, T. N., &Miyake, K. (2011). Causes of catastrophic failure of Tam Pokhari moraine dam in the Mt. Everest region, Natural Hazards, 58(3), 1209-1223, https://doi:10.1007/s11069-011-9723-x.
Otto, J.-C. (2019). Proglacial Lakes in High Mountain Environments, in Geomorphology of Proglacial Systems, edited, pp. 231-247, https://doi:10.1007/978-3-319-94184-4_14.
Pang, Q., Zhao, L., Li, S., &Ding, Y. (2011). Active layer thickness variations on the Qinghai–Tibet Plateau under the scenarios of climate change, Environmental Earth Sciences, 66(3), 849-857, https://doi:10.1007/s12665-011-1296-1.
Qin, Y., et al. (2017). Numerical Modeling of the Active Layer Thickness and Permafrost Thermal State Across Qinghai-Tibetan Plateau, Journal of Geophysical Research: Atmospheres, 122(21), 11,604-611,620, https://doi:10.1002/2017jd026858.
Rajaure, S., Paudyal, K. R., &Dahal, P. R. (2018). Geophysical study on moraine dam of Imja Glacial Lake in Eastern Nepal using Electrical Resistivity Tomography Method, Journal of Nepal Geological Society, 55(1), 15-22, https://doi:10.3126/jngs.v55i1.22784.
Riseborough, D., Shiklomanov, N., Etzelmüller, B., Gruber, S., &Marchenko, S. (2008). Recent advances in permafrost modelling, Permafrost and Periglacial Processes, 19(2), 137-156, https://doi:10.1002/ppp.615.
Riseborough, D. W. (2004). Exploring the parameters of a simple model of the permafrost-climate relationship, Carleton University.
Rounce, D. R., McKinney, D. C., Lala, J. M., Byers, A. C., &Watson, C. S. (2016). A new remote hazard and risk assessment framework for glacial lakes in the
Nepal Himalaya, Hydrology and Earth System Sciences, 20(9), 3455-3475, https://doi:10.5194/hess-20-3455-2016.
Saito, K., Kimoto, M., Zhang, T., Takata, K., &Emori, S. (2007). Evaluating a high-resolution climate model: Simulated hydrothermal regimes in frozen ground regions and their change under the global warming scenario, Journal of Geophysical Research, 112(F2), https://doi:10.1029/2006jf000577.
Staub, B., &Delaloye, R. (2017). Using Near-Surface Ground Temperature Data to Derive Snow Insulation and Melt Indices for Mountain Permafrost Applications, Permafrost and Periglacial Processes, 28(1), 237-248, https://doi:10.1002/ppp.1890.
Su, P. F., Wang, W. M., He, J., &Chen, S. H. (2009). Integrated simulation and safety assessment for RCC gravity dam on rock foundation during whole process of construction, Rock & Soil Mechanics, 30(6), 1769-1774, https://doi:10.1109/MILCOM.2009.5379889.
Tan, X., Chen, W., HongmingTian, &Cao, J. (2011). Water flow and heat transport including ice/water phase change in porous media: Numerical simulation and application, Cold Regions Science & Technology, 68(1-2), p.74-84, https://doi:10.1016/j.coldregions.2011.04.004.
Taylor, G. S., &Luthin, J. N. (1978). A model for coupled heat and moisture transfer during soil freezing, Revue Canadienne De Géotechnique, 15(4), 548-555, https://doi:10.1139/t78-058.
Thompson, S., Kulessa, B., &Luckman, A. (2012). Integrated electrical resistivity tomography (ERT) and self-potential (SP) techniques for assessing hydrological processes within glacial lake moraine dams, Journal of Glaciology, 58(211), 849-858, https://doi:10.3189/2012JoG11J235.

Tofani, V., Raspini, F., Catani, F., &Casagli, N. (2013). Persistent Scatterer Interferometry (PSI) Technique for Landslide Characterization and Monitoring, Remote Sensing, 5(3), 1045-1065, https://doi:10.3390/rs5031045.

Wang, H. B., Qiang, S., Sun, X., &Zheng, R. (2011). Dynamic Simulation Analysis of Temperature Field and Thermal Stress of Concrete Gravity Dam during Construction Period, Applied Mechanics and Materials, 90-93, https://doi:10.4028/www.scientific.net/AMM.90-93.2677.

Wang, W., Zhang, T., Yao, T., &An, B. (2022). Monitoring and early warning system of Cirenmaco glacial lake in the central Himalayas, International Journal of Disaster Risk Reduction, 73, https://doi:10.1016/j.ijdrr.2022.102914.

Wang, X., Liu, Q., Liu, S., &He, G. (2021). Manifestations and mechanisms of mountain glacier-related hazards, Sciences in Cold and Arid Regions, 12, 436-446, https://doi:10.3724/SP.J.1226.2020.00436.

Wang, X., Liu, S., Ding, Y., Guo, W., Jiang, Z., Lin, J., &Han, Y. (2012). An approach for estimating the breach probabilities of moraine-dammed lakes in the Chinese Himalayas using remote-sensing data, Natural Hazards and Earth System Sciences, 12(10), 3109-3122, https://doi:10.5194/nhess-12-3109-2012.

Wang, X., Liu, S., Guo, W., &Xu, J. (2008). Assessment and Simulation of Glacier Lake Outburst Floods for Longbasaba and Pida Lakes, China, Mountain Research and Development, 28(3/4), 310-317, https://doi:10.1659/mrd.0894.

Wang, X., Yang, C., Zhang, Y., Chai, K., Liu, S., Ding, Y., Wei, J., Zhang, Y., &Han, Y. (2018). Monitoring and simulation of hydrothermal conditions indicating the deteriorating stability of a perennially frozen moraine dam in the Himalayas, Journal of Glaciology, 64(245), 407-416, https://doi:10.1017/jog.2018.38.

Wei, C., Yu, S., Jichun, W., Yaling, C., Erxing, P., &Leonid, G. (2021). Soil hydrological process and migration mode influenced by the freeze-thaw process in the activity layer of permafrost regions in Qinghai-Tibet Plateau, Cold Regions Science and Technology, 184, https://doi:10.1016/j.coldregions.2021.103236.

Westoby, M. J., Glasser, N. F., Brasington, J., Hambrey, M. J., Quincey, D. J., &Reynolds, J. M. (2014). Modelling outburst floods from moraine-dammed glacial lakes, Earth-Science Reviews, 134, 137-159, https://doi:10.1016/j.earscirev.2014.03.009.

Worni, R., Stoffel, M., Huggel, C., Volz, C., Casteller, A., &Luckman, B. (2012). Analysis and dynamic modeling of a moraine failure and glacier lake outburst flood at Ventisquero Negro, Patagonian Andes (Argentina), Journal of Hydrology, 444-445, 134-145, https://doi:10.1016/j.jhydrol.2012.04.013.

Wu, Q., Zhang, T., &Liu, Y. (2012). Thermal state of the active layer and permafrost along the Qinghai-Xizang (Tibet) Railway from 2006 to 2010, The Cryosphere, 6(3), 607-612, https://doi:10.5194/tc-6-607-2012.

Wu, X., Nan, Z., Zhao, S., Zhao, L., &Cheng, G. (2018). Spatial modeling of permafrost distribution and properties on the Qinghai-Tibet Plateau, Permafrost and Periglacial Processes, 29(2), 86-99, https://doi:10.1002/ppp.1971.

Yan, Z., Pan, W., Fang, J., Liu, Z., &Zhao, Y. (2020). Numerical Simulation of Thawing Process in Frozen Soil, Geofluids, 2020, 1-7, https://doi:10.1155/2020/8822320.

Yao, T., Li, Z., Yang, W., Guo, X., Zhu, L., Kang, S., Wu, Y., &Yu, W. (2010). Glacial distribution and mass balance in the Yarlung Zangbo River and its influence on lakes, Chinese Science Bulletin, 55(20), 2072-2078, https://doi:10.1007/s11434-010-3213-5.

Yao, X., Liu, S., Sun, M., Wei, J., &Guo, W. (2012). Volume calculation and analysis of the changes in moraine-dammed lakes in the north Himalaya: a case study of Longbasaba lake, Journal of Glaciology, 58(210), 753-760, https://doi:10.3189/2012JoG11J048.

Zhang, M., Min, K.-H., Wu, Q., Zhang, J., &Harbor, J. (2012). A New Method to Determine the Upper Boundary Condition for a Permafrost Thermal Model: An Example from the Qinghai-Tibet Plateau, Permafrost and Periglacial Processes, 23(4), 301-311, https://doi:10.1002/ppp.1755.

Zhang, M., Wang, J., &Lai, Y. (2019). Hydro-thermal boundary conditions at different underlying surfaces in a permafrost region of the Qinghai-Tibet Plateau, Sci Total Environ, 670, 1190-1203, https://doi:10.1016/j.scitotenv.2019.03.090.

Zhang, M. L., Guo, Z. Y., Han, X. B., Wang, B., Wei, H. T., &Gao, Q. (2018). Analysis of Coupled Water and Heat Transfer in Frozen Soil Based on Mathematical Module of COMSOL Multiphysics, Science Technology and Engineering.

Zhang, T., Barry, R. G., Knowles, K., &Heginbottom, J. A. (2008). Statistics and characteristics of permafrost and ground-ice distribution in the Northern Hemisphere: Polar Geography: Vol 31, No 1-2, Polar Geography, https://doi:10.1080/10889370802175895.

Zhao, L., Ren, L. I., &Ding, Y. J. (2008). Simulation on the Soil Water-Thermal Characteristics of the Active Layer in Tanggula Range, Journal of Glaciology and Geocryology, https://doi:10.1007/s11442-008-0201-7.

Zhao, Y., Si, B., He, H., Xu, J., Peth, S., &Horn, R. (2016). Modeling of Coupled Water and Heat Transfer in Freezing and Thawing Soils, Inner Mongolia, Water, 8(10), https://doi:10.3390/w8100424.

Zheng, G., et al. (2021). Increasing risk of glacial lake outburst floods from future Third Pole deglaciation, Nature Climate Change, 11(5), 411-417, https://doi:10.1038/s41558-021-01028-3.

Zou, D., Zhao, L., Sheng, Y., Chen, J., &Cheng, G. (2017). A new map of permafrost distribution on the Tibetan Plateau, The Cryosphere, 11(6), 2527-2542, https://doi:10.5194/tc-11-2527-2017.